Nuclear Engineering and Technology 52 (2020) 148–154

Contents lists available at ScienceDirect

Nuclear Engineering and Technology

journal homepage: www.elsevier.com/locate/net

Original Article

Radiation induced grain boundary segregation in ferritic/martensitic steels

L.D. Xia [a], Y.Z. Ji [b], W.B. Liu [c], H. Chen [a], Z.G. Yang [a], C. Zhang [a, *], L.-Q. Chen [b]

[a] Key Laboratory of Advanced Materials of Ministry of Education, School of Materials Science and Engineering, Tsinghua University, Beijing, 100084, China
[b] Department of Materials Science and Engineering, The Pennsylvania State University, University Park, PA, 16802, USA
[c] Department of Nuclear Science and Technology, Xi'an Jiaotong University, Xi'an, 710049, China

ARTICLE INFO

Article history:
Received 19 February 2019
Received in revised form
11 June 2019
Accepted 9 July 2019
Available online 9 July 2019

Keywords:
Radiation induced segregation
Ferritic/martensitic
Temperature
Grain boundary structure

ABSTRACT

The radiation induced segregation of Cr at grain boundaries (GBs) in Ferritic/Martensitic steels was modeled assuming vacancy and interstitialcy diffusion mechanisms. In particular, the dependence of segregation on temperature and grain boundary misorientation angle was analyzed. It is found that Cr enriches at grain boundaries at low temperatures primarily through the interstitialcy mechanism while depletes at high temperatures predominantly through the vacancy mechanism. There is a crossover from Cr enrichment to depletion at an intermediate temperature where the Cr:Fe vacancy and interstitialcy diffusion coefficient ratios intersect. The bell-shape Cr enrichment response is attributed to the decreasing void sinks inside the grains as temperature rises. It is also shown that low angle grain boundaries (LAGBs) and special Σ coincidence-site lattice (CSL) grain boundaries exhibit suppressed radiation induced segregation (RIS) response while high angle grain boundaries (HAGBs) have high RIS segregation. This different behavior is attributed to the variations in dislocation density at different grain boundaries.

1. Introduction

Ferritic/Martensitic (F/M) steels are leading candidate structural materials for the next generation of fusion and fission nuclear reactors [1–3]. F/M steels show high strength, low swelling, resistance to thermal stress and corrosion under irradiation [4]. However, F/M steels have been shown to be susceptible to radiation induced segregation (RIS) of Cr at grain boundaries. Cr enrichment may enhance precipitation, which could lead to embrittlement, whereby Cr depletion may dramatically alter the corrosion resistance of grain boundaries [5].

RIS has been extensively studied in the past decades. The RIS behavior of Cr in austenitic steels is relatively well-understood [6], where Cr depletion is always observed at grain boundaries. But in F/M steels, RIS has not yet been well understood. Lu et al. [7] summarized the limited experimental literatures, and found that out of the total 15 published results, eight showed Cr enrichment and seven showed Cr depletion. However, it is difficult to draw a clear conclusion on the tendency towards enrichment or depletion of Cr because these results are from different materials and conditions. Was and Wharry et al. [8,9] have recently done systematic studies and observed that for given F/M steels and irradiation conditions, RIS of Cr has a bell-shape temperature dependence, changing from Cr enrichment to Cr depletion at grain boundaries with increasing temperatures. In addition to temperature dependence, recent studies also showed variation in Cr segregation from boundary to boundary in samples under the same irradiation conditions [10–12]. The results showed that low angle grain boundaries (LAGB) exhibited a suppressed RIS response when compared to relatively high angle grain boundaries (HAGB), and at the special Σ CSL boundaries, the RIS of Cr was also suppressed.

Several theoretical models have been proposed to describe RIS. RIS in austenitic steels has been firstly and extensively studied. The first model was developed by Johnson and Lam [13], and then Marwick [14–16], Okamoto [17], Wiedersich [18], Murphy and Perks [19–22] made modifications from different perspectives. Allen and Was [23–25] extended the model to ternary system and applied it to Fe–Cr–Ni alloy. Watanabe [26], Duh [27] and Field et al. [28] incorporated a grain boundary absorption strength term into the model to study the effect of grain boundary structures on RIS in austenitic steels. So far, theoretical models for RIS in

* Corresponding author.
E-mail address: chizhang@tsinghua.edu.cn (C. Zhang).

https://doi.org/10.1016/j.net.2019.07.009

austenitic steels have been developed quite well. As for F/M steels, however, not much work has been done. Wharry and Was [29] found that, unlike austenitic steels, self-interstitials played an important role in RIS in F/M steels. Cr enrichment is mainly attributed to self-interstitials at low temperatures, and Cr depletion is caused by vacancies at high temperatures. Field et al. [12] recently studied the effect of grain boundary structures on RIS in F/M steels.

However, existing RIS theories have not considered the defect-void interactions, which may play an important role in the bell-shape temperature dependence. Furthermore, to our knowledge, the dependence of the RIS response on grain boundary characteristics in F/M steels has not been investigated in details. This study attempts to develop a RIS model, in which the defect-void interaction as well as the effect of grain boundary structures are considered.

2. Model description

The purpose of this section is to describe the modeling methodology, and for simplicity, we consider the Fe–Cr binary system as model system for the F/M steels for understanding the basic mechanisms of RIS.

2.1. Governing equations

RIS is due to the fluxes of self-interstitials and vacancies towards grain boundaries which, in the Fe–Cr alloy, induce fluxes of Fe and Cr, as shown in Fig. 1. Thus, in the present work, it is assumed that the flux of Fe or Cr is determined by its partial diffusion via vacancy and interstitialcy diffusion mechanisms [30]. The differential rate equations of atoms (Fe and Cr) and defects (vacancy and interstitial, subscript v and i in Eq. (2), respectively) are written as

$$\frac{\partial C_k}{\partial t} = -\nabla \cdot J_k \quad (k = Fe,\ Cr) \tag{1}$$

$$\frac{\partial C_{v,i}}{\partial t} = -\nabla \cdot J_{v,i} + P_{v,i} - K_{v,i} - S_{v,i} \tag{2}$$

where C is the mole fraction of the species of interest, J is the diffusion flux, and P, K and S are production rate, recombination rate and sink absorption rate of vacancy and self-interstitial respectively. The fluxes of the defects and solute atoms are

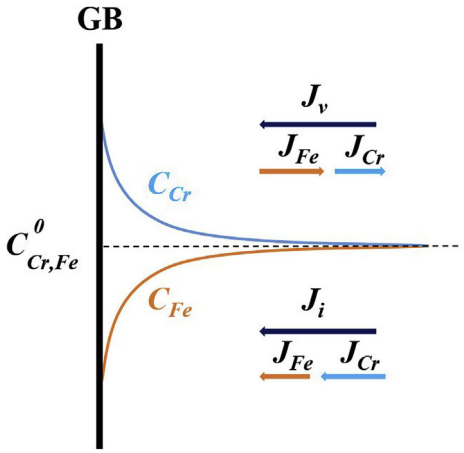

Fig. 1. Schematic of radiation induced segregation in Fe–Cr F/M steels.

$$J_v = J_v^{Fe} + J_v^{Cr} \tag{3}$$

$$J_i = J_i^{Fe} + J_i^{Cr} \tag{4}$$

$$J_k = J_k^{v} + J_k^{i} \tag{5}$$

$$J_v^k (\equiv -J_k^v) = d_k^v (C_v \nabla C_k - C_k \nabla C_v) \tag{6}$$

$$J_i^k \left(\equiv J_k^i\right) = d_k^i (-C_i \nabla C_k - C_k \nabla C_i) \tag{7}$$

where $J_v^k (J_i^k)$ is the partial vacancy (interstitial) flux via k atom, $J_k^v (J_k^i)$ is the partial flux of k atom via vacancy (interstitial). $d_k^v (d_k^i)$ is the diffusivity coefficient for the atom-defect pairs, and is determined by

$$d_k^{v,i} = \frac{1}{6}\lambda^2 \omega f exp\left(-\frac{E_{k-v,i}^m}{k_B T}\right) \tag{8}$$

where λ is the jump distance, ω is the jump frequency for a k atom to diffuse via the vacancy or interstitialcy mechanism, f is the correlation factor [29], $E_{k-v,i}^m$ is the migration energy of the vacancy or interstitial and k_B is the Boltzmann constant.

2.2. Defects generation and recombination

In the present work, we assume that the vacancies and interstitials have the same generation rate, which is 1×10^{-5}/s. The recombination rate is the same for both vacancies and interstitials since they must recombine with each other at the same rate. The recombination rate of vacancies and interstitials used in this work is the same as that in reference [30], $K_{iv} = \frac{500\Omega(D_i + D_v)C_i C_v}{a^2}$, where Ω is the atomic volume and a is the lattice parameter.

2.3. Sink terms

The key difference between the present work and previous RIS models for F/M steels is the treatment of the sink terms. Few of the previous models have taken the defect-void interaction into consideration, but after irradiation there are high density of voids in F/M steels [31], which means the absorption of defects by voids is not negligible. Moreover, in most other models, the grain boundaries are treated as ideal sinks, which can hardly explain the variation in Cr segregation from boundary to boundary. In this work, the defect-void interaction and an alternative grain boundary condition are taken into account.

2.3.1. Void absorption

Consider the case of ρ_V voids per unit volume with radius r_0, which absorb point defects present in the solid and between the spherical sinks. Was [30] has calculated the absorption rate with detailed derivation, which is briefly outlined here. Focusing on a single sphere, the radius R of the capture volume around each sphere is defined by

$$\left(\frac{4}{3}\pi R^3\right)\rho_V = 1 \tag{9}$$

The diffusion equation of the point defects could be solved in the spherical shell $r_0 \le r \le R$, the local equilibrium solution is given as

$$C(r) = C_{r0} + [C_R - C_{r0}]\left[1 - \frac{r_0}{r}\right] \quad (10)$$

where C_{r0} equals to the thermal equilibrium point defect concentration, which is much lower than C, then the absorption rate per unit volume could be calculated by

$$S = 4\pi r_0^2 \rho_V J_{r_0} = 4\pi r_0^2 \rho_V D\left(\frac{dC}{dr}\right)_{r_0} = 4\pi r_0 D \rho_V C \quad (11)$$

Therefore, the absorption rate of vacancies and interstitials by voids is calculated by $S_{v-V} = 4\pi r_0 D_v \rho_V C_v$ and $S_{i-V} = 4\pi r_0 D_i \rho_V C_i$.

2.3.2. Grain boundary absorption

As for grain boundary, we assume its sink strength is a function of grain boundary misorientation angle, where a general high misorientation angle leads to a high sink strength, while a low misorientation angle or misorientation near high angle coincidence-site lattice (CSL) boundaries lead to a low sink strength. Duh et al. [27] described the grain boundary as a pure symmetric tilt boundary consisting of an array of parallel dislocations, and it is assumed that individual dislocations comprising a grain boundary are perfect sinks for defects.

Consider such a case, the Burgers vector of dislocations comprising the grain boundary is b and the distance between the dislocations is d, the radius of the capture volume around each dislocation is defined as $d/2$. The diffusion equation of the point defects could be solved in cylindrical geometry and the solution is given as [30].

$$C(r) = C_b + \left[C_{d/2} - C_b\right]\frac{ln(r/b)}{ln(d/2b)} \quad (12)$$

where C_b equals to the thermal equilibrium defect concentration, which is much lower than C, then the absorption rate of the grain boundary could be calculated as

$$S_{gb} = \frac{2\pi b J_b}{d^2} = \frac{2\pi b D}{d^2}\left(\frac{dC}{dr}\right)_b = \frac{2\pi D C}{d^2 ln(d/2b)} \quad (13)$$

Therefore, the absorption rate of vacancies and interstitials by grain boundaries is calculated by $S_{v-gb} = \frac{2\pi D_v C_v}{d^2 ln(d/2b)}$ and $S_{i-gb} = \frac{2\pi D_i C_i}{d^2 ln(d/2b)}$.

In order to study RIS behavior as a function of grain boundary misorientation angle, it is necessary to describe the grain boundary absorption strength in terms of grain boundary misorientation angle. According to the theory proposed by Brandon [32], a grain boundary with misorientation angle θ can be described with the value of Σ and a deviation angle $\Delta\theta$, where $\Delta\theta = \theta - \theta_{CSL}$. For example, the angle of a $\Sigma 3$ CSL boundary is 60°, then the grain boundary with θ of 63° can be describe with ($\Sigma = 3$, $\Delta\theta = 3°$). The length of Burgers vectors b of the grain boundary dislocations in Σ-boundary may be approximated as [27].

$$b = a/\sqrt{\Sigma} \quad (14)$$

where a is the lattice parameter, and the distance between the dislocations can be given as

$$d = \frac{b}{2sin\left(\frac{\Delta\theta}{2}\right)} \quad (15)$$

Because the grain boundary absorption strength is a function of Burgers vector b and distance d, we know the relationship between grain boundary absorption strength and misorientation angle θ.

2.4. Input parameters

Most of the input parameters were selected to be consistent with previous study for a F/M Fe–9Cr alloy and are given in Table 1. These values were taken from experiments or model simulations [29,31,33,34].

3. Simulation results

One-dimension calculations were performed. Fourier-spectral method was used to solve the governing equations with periodic boundary conditions and the grain boundary was put in the middle of the simulation domain. The system size for the simulation is $128\Delta x$ with grid size $\Delta x = 1\ nm$, and the grain boundary is characterized by $1\Delta x$. The time step is $dt = 10^{-10}\ s$. In this section, model calculations will be compared with the experimental measurements presented in Ref. [8,12]. It is necessary to figure out which behaviors are important to the comparison. In the Ref. [8,12], two distinct features of Cr RIS behaviors were presented: (1) a bell-shape temperature dependence and a crossover from Cr enrichment to Cr depletion, (2) LAGBs exhibit a suppressed RIS response when compared to HAGBs, and at the Σ CSL boundaries, the RIS of Cr is also suppressed.

3.1. Temperature dependence

The calculation results showed a crossover from Cr enrichment to Cr depletion as temperature rose, in which Cr enrichment occurred at grain boundary when temperatures were below 640 °C,

Table 1
Input parameters used in the Fe–Cr RIS model.

Input parameter	Symbol	Unit	Value	Reference
Lattice parameter	a	m	2.87×10^{-10}	[31]
Vacancy jump frequency for Fe	ω_{Fe-v}	s^{-1}	1.60×10^{13}	[33]
Vacancy jump frequency for Cr	ω_{Cr-v}	s^{-1}	2.40×10^{13}	[33]
Interstitial jump frequency for Fe	ω_{Fe-i}	s^{-1}	2.90×10^{13}	[34]
Interstitial jump frequency for Cr	ω_{Cr-i}	s^{-1}	4.20×10^{13}	[34]
Vacancy migration energy for Fe	E^m_{Fe-v}	eV	0.61	[29]
Vacancy migration energy for Cr	E^m_{Cr-v}	eV	0.55	[29]
Interstitial migration energy for Fe	E^m_{Fe-i}	eV	0.35	[29]
Interstitial migration energy for Cr	E^m_{Cr-i}	eV	0.28	[29]
Vacancy jump correlation factor for Fe	$f_{v\ Fe}$	unitless	0.727	[29]
Vacancy jump correlation factor for Cr	$f_{v\ Cr}$	unitless	0.797	[35]
Interstitial jump correlation factor for Fe	$f_{i\ Fe}$	unitless	0.727	[29]
Interstitial jump correlation factor for Cr	$f_{i\ Cr}$	unitless	0.727	[29]

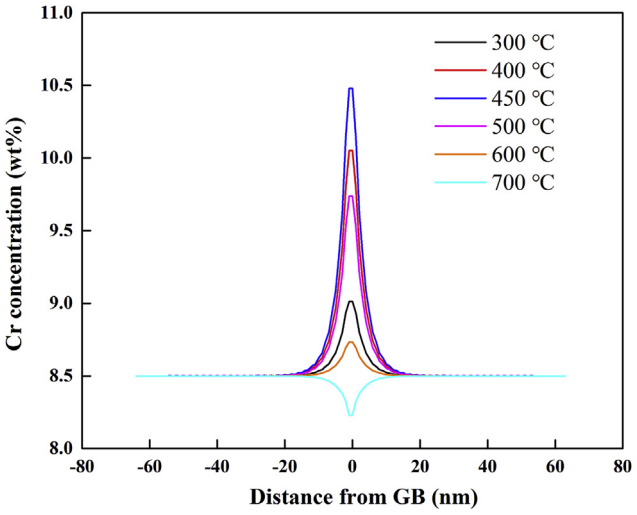

Fig. 2. Amount of Cr RIS at the irradiation temperature from 300 °C to 700 °C.

and Cr depletion occurred at temperatures above 640 °C.

This simulation also exhibited a bell-shape temperature dependence of RIS, where the Cr enrichment is suppressed at low and high temperatures, and maximized at a moderate temperature. As shown in Fig. 2, when the temperature increases from 300 °C to 700 °C, the Cr enrichment increases first and reaches maximum at 450 °C, and then decreases until changing from Cr enrichment to Cr depletion at 640 °C. These behaviors are similar to the experimental results in Ref. [8], as shown in Fig. 3.

3.2. Grain boundary dependence

The dependence of Cr RIS on grain boundary structure was calculated at 400 °C. The calculation results in Fig. 4 showed that as the misorientation angle increases from LAGBs to HAGBs, the Cr enrichment at grain boundary increases monotonically and HAGBs exhibit the largest magnitude of Cr enrichment. However, as shown in Fig. 5 not all HAGBs exhibit high Cr enrichment and several special grain boundaries show suppressed Cr enrichment. The Σ3 and Σ5 CSL grain boundaries exhibited similar behaviors of Cr

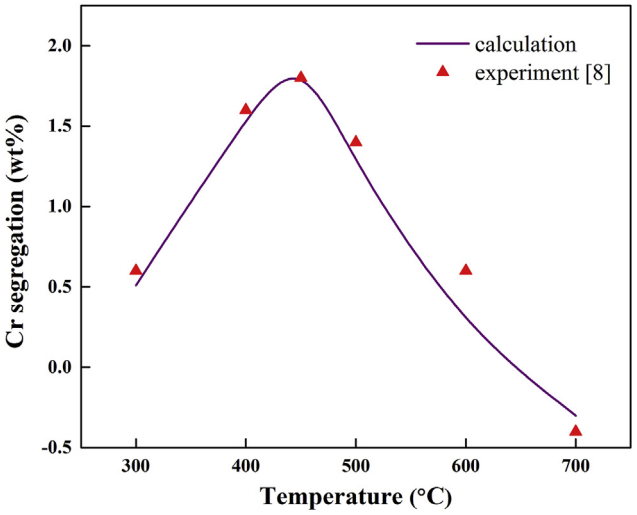

Fig. 3. Comparison of temperature dependence of RIS between calculation and experimental results.

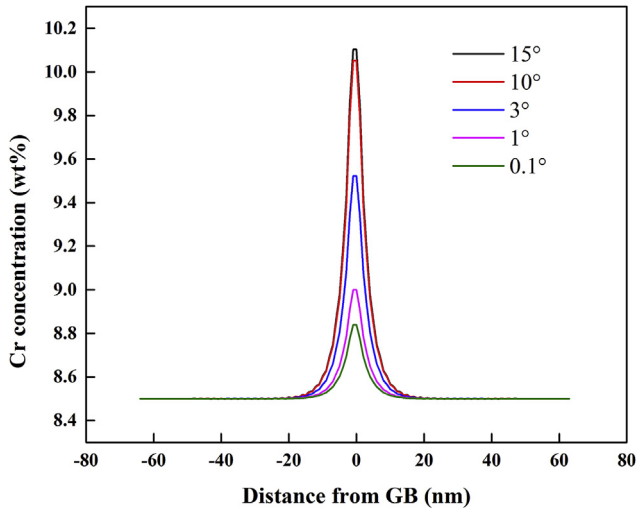

Fig. 4. The Cr RIS enrichment response when changing from LAGBs to HAGBs at 400 °C.

enrichment to the LAGBs. As the deviation angle increased, the RIS response increased until it was like the other general HAGBs.

4. Discussion

4.1. Temperature dependence

The calculation results above showed two temperature dependence behaviors, one is the crossover from Cr enrichment to Cr depletion at about 640 °C, and another is a bell-shape temperature dependence of RIS, where Cr enrichment is suppressed at low and high temperatures, and maximized at a moderate temperature.

RIS originates from coupling between point defects flux and alloy elements flux towards grain boundaries [30]. When a steady state is reached, the relation between Cr atom concentration gradient and vacancy concentration gradient is [30]:

$$\nabla C_{Cr} = \frac{N_{Cr}N_{Fe}d_{Cr}^{i}d_{Fe}^{i}}{d_{Cr}^{i}N_{Cr}D_{Fe} + d_{Fe}^{i}N_{Fe}D_{Cr}}\left(\frac{d_{Cr}^{v}}{d_{Fe}^{v}} - \frac{d_{Cr}^{i}}{d_{Fe}^{i}}\right)\nabla C_{v} \quad (16)$$

It is evident that the relation between the direction of Cr atom

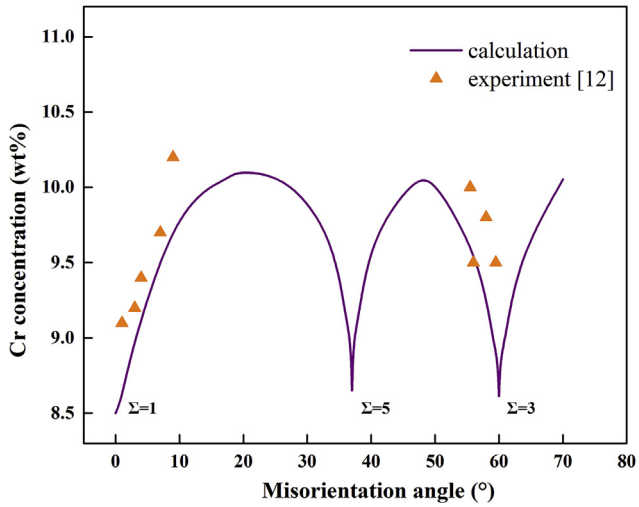

Fig. 5. Amount of Cr RIS as a function of misorientation angle.

concentration gradient and vacancy concentration gradient is determined by the ratios $\frac{d_{Cr}^{v}}{d_{Fe}^{v}}$ and $\frac{d_{Cr}^{i}}{d_{Fe}^{i}}$. During irradiation, vacancies and interstitials annihilate at grain boundaries. The vacancy concentration always decreases towards a grain boundary. Therefore, Eq. (16) predicts that Cr enriches at grain boundaries when $\frac{d_{Cr}^{v}}{d_{Fe}^{v}} < \frac{d_{Cr}^{i}}{d_{Fe}^{i}}$, which means the contribution of Cr enrichment by interstitials dominates the contribution of Cr depletion by vacancies, resulting in a net Cr enrichment. Conversely, Cr depletes when $\frac{d_{Cr}^{v}}{d_{Fe}^{v}} > \frac{d_{Cr}^{i}}{d_{Fe}^{i}}$, which means Cr depletion by vacancies dominates Cr enrichment by interstitials, resulting in a net Cr depletion. As shown in Fig. 6, the Cr:Fe vacancy diffusion coefficient ratio, as calculated from Eq. (8), crossed interstitialcy diffusion coefficient ratio at 640 °C. Hence for temperatures below 640 °C, interstitialcy diffusion dominated and Cr enriched, and for temperature above 640 °C, vacancy diffusion dominated and Cr depleted at grain boundaries. In Fe–Cr austenitic steels, only Cr depletion is observed because RIS in austenitic steels is mainly driven by vacancies while interstitials do not contribute significantly [23,24].

Wharry and Was [29,35] have found that simulation results would be in better agreement with experimental measurements when other sinks inner the grain are considered, such as dislocation loops, carbides and voids. However, there remain discrepancies between calculation and experimental results. One difference is that the calculation result could hardly explain the bell-shape temperature dependence. This difference is likely because irradiation temperature could change the inner sink strength, which in the previous models always given a constant value as temperature changes. Ref. [31] has shown that the densities and sizes of voids in a F/M alloy irradiated at 200 °C and 350 °C are $1.1 \times 10^{25}\ m^{-3}$, $1.5 \times 10^{24}\ m^{-3}$ and 1.2 nm, 2.3 nm respectively, and voids are the most dominant sinks inner the grain. In the above section, Eq. (11) gives the void sink strength and it denotes that the strength is proportional to the product of density and size of voids, which is $4\pi r_0 \rho_V$. With the void sizes and densities in reference [31], the calculated void sink strength is 0.067 m^{-2}, 0.027 m^{-2}, 0.017 m^{-2}, 0.011 m^{-2}, 0.004 m^{-2} and 0.002 m^{-2} at temperature 300 °C, 400 °C, 450 °C, 500 °C, 600 °C, 700 °C, respectively. The results show that as temperature rises, the void sink strength decreases. Fig. 7 shows the Cr RIS with constant void sink strength. When the void sink strength is constant, Cr enriches at low temperatures and the enrichment magnitude decreases monotonically with increasing temperature, which is not in agreement with the bell-shape temperature dependence observed in experiments. However, when introducing a variable void sink strength, which decreases as temperature rises, Cr enrichment is suppressed at low and high temperatures, and reaches a maximum at a moderate temperature. Eq. (16) shows that both the difference between the vacancy and interstitial diffusivity ratios and the gradient of vacancy near the grain boundary contribute to the Cr RIS. When the void sink strength is constant, the rising temperature leads to a much faster mobility of defects, resulting in a higher vacancy and interstitial recombination rate. The higher recombination reduces the vacancy flux to grain boundaries, and hence, the gradient of vacancy near the grain boundaries decreases, as shown in Fig. 8(a). Therefore, the reduction in the magnitude of gradient of vacancy as well as the reduction of the difference between the vacancy and interstitial diffusivity ratios results in a monotonically decreasing Cr RIS as temperature rises, as shown in Fig. 7, which has been done in Ref. [35]. However, when a decreasing void sink strength with temperature is introduced in this work, as temperature rises, the decreasing void sink would offset the increasing defect mobility and restrain the recombination rate. This leads to an increasing gradient of vacancy near the grain boundary, as shown in Fig. 8(b). When the temperature is above 500 °C, the vacancy gradient drops slightly. This may be attributed to the reason that the decreasing strength cannot compensate for the increasing mobility of defects, because there exists a lower limit for the void sink strength to decrease. The collective effect of increasing vacancy gradient and decreasing difference between the vacancy and interstitial diffusivity ratios leads to a bell-shape temperature dependence. At the same temperature, with the increase of radiation dose (radiation time), the void sizes and density also evolve, which means the void sink strength changes. However, in this model, we used a constant void sink strength during the establishment of the steady state of RIS, because the evolution of void size and density is much slower than the establishment of the steady state of RIS. According to reference [31], when irradiated for 2 h at 200 °C, the void size and density in the F/M steel are 1.2 nm and $\sim 1.1 \times 10^{25}\ /m^3$, and when irradiated for 8 h at 200 °C, the void size and density are 1.7 nm and $\sim 1.6 \times 10^{25}\ /m^3$, we can find that the evolution of void size and density is quite slow. As a contrast, our calculation result shows that the establishment of the steady state of RIS takes less than 150 μs, as shown in Fig. 9.

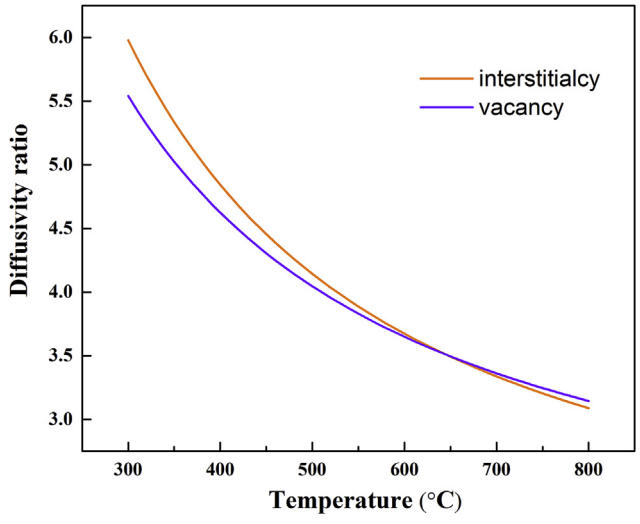

Fig. 6. The dependence of vacancy and interstitialcy diffusion coefficient ratios for Fe–Cr F/M steels on temperature.

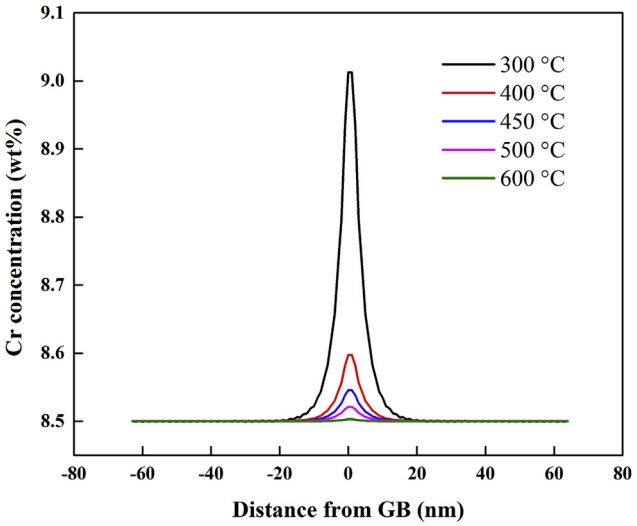

Fig. 7. The Cr RIS response without including a variable void sink strength.

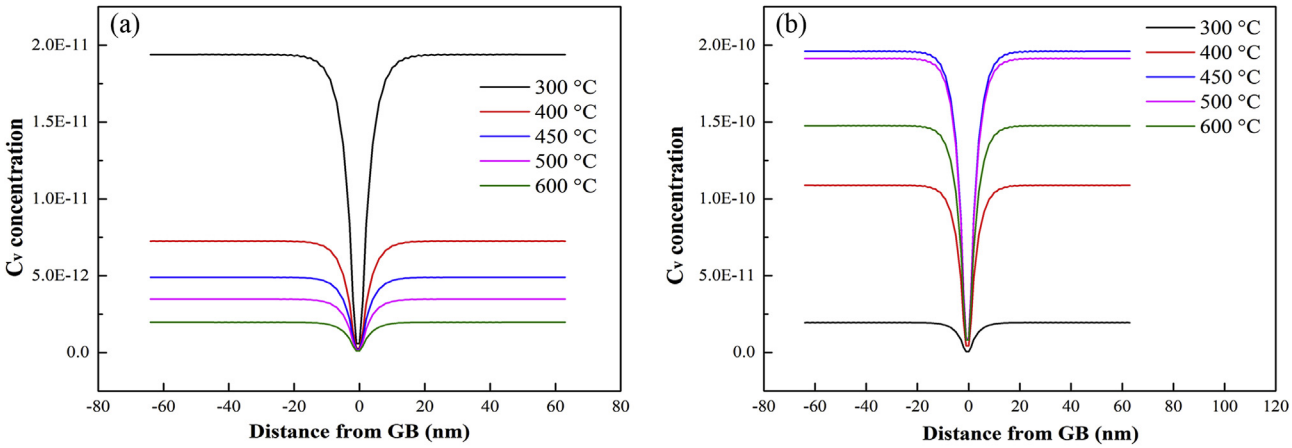

Fig. 8. Concentration of vacancies near the grain boundaries at 400 °C, (a) with constant void sink strength, (b) with variable void sink strength.

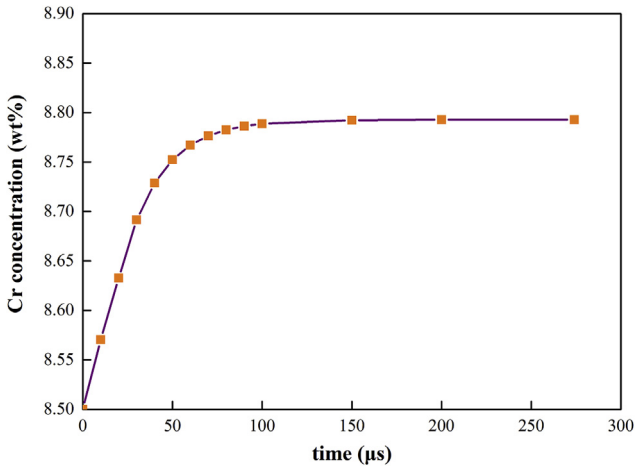

Fig. 9. Evolution of Cr concentration at grain boundaries under irradiation at 200 °C.

4.2. Grain boundary dependence

The calculation results above showed that the Cr enrichment increased as the misorientation angle increased from LAGBs to HAGBs, and the Σ3 and Σ5 CSL grain boundaries exhibited similar behaviors of Cr enrichment to the LAGBs. This is because the sink strength depends on the misorientation angle. Some of the previous work treated the grain boundary as perfect sink for point defects, which assumes the point defects always maintain equilibrium concentration at grain boundaries. This treatment ignores the effect of grain structure on sink strength. A better treatment is to assume that grain boundaries consist of an array of dislocations and these dislocations act as perfect sinks for point defects [12,27,28]. Eq. (13–15) show the relationship between sink strength and misorientation angle. When it changes from LAGBs to HAGBs, the dislocation density at grain boundaries increases rapidly with increasing misorientation and it strengthens the annihilation of point defects, resulting in a larger gradient of vacancy concentration near grain boundary. Therefore, it leads to increasing Cr RIS enrichment with misorientation.

However, not all HAGBs exhibited high Cr RIS response. For example, our calculation results showed Σ3 and Σ5 CSL grain boundaries had similar behaviors of Cr response to the LAGBs. This is because some HAGBs are special Σ CSL grain boundaries, and their high degree of order results in a pretty low concentration of grain boundary dislocations, as implied in Eq. (15). Based on the Brandon criterion [36], the grain boundary with a deviation angle from the exact CSL orientation could be calculated. The minimum amount of RIS segregation occurred at the exact Σ CSL orientation, and increasing segregation could be observed with increasing deviation from the exact Σ CSL orientation, which results from the increase in the density of grain boundary dislocations implied by the Brandon criterion. The similar RIS response behavior between the Σ CSL grain boundaries and LAGBs is because that LAGBs actually are grain boundaries deviated from Σ1 CSL orientation. Therefore, LAGBs have the similar performance as other Σ CSL grain boundaries, such as Σ3 and Σ5.

This method shows that simulation results are in general agreement with experimental results and it confirms the validity of using this approach to help understand RIS in F/M steels. However, several limitations still exist. The model took only orientation angle to describe grain boundary structure. This is just one-degree parameterization out of the five parameters to describe a grain boundary. Further work would be needed to take the effect of grain boundary plane and misorientation axis into account to include all possible degrees of freedom. Also, this model applies to a simple Fe–Cr binary system, whereas additional work would be needed to understand the role of impurities and other minor alloy elements in RIS in F/M steels.

5. Conclusion

The behavior of Cr RIS in F/M steels was investigated with a modified model based on previous works. The dependence of RIS on temperature and grain boundary characteristics was reproduced.

The temperature dependence of Cr RIS is attributed to the collective contribution of vacancies and interstitials. At low temperatures, the contribution of Cr enrichment by interstitials dominates, resulting in a Cr enrichment. At high temperatures, Cr depletion by vacancies dominates, resulting in a Cr depletion. Therefore, there is a crossover from enrichment to depletion at a moderate temperature. As temperature rises, the difference between the vacancy and interstitial diffusivity ratios decreases; meanwhile, the void sink strength decreases, leading to an increasing vacancy gradient near grain boundaries. Their collective effect results in the bell-shape Cr RIS enrichment response.

LAGBs and Σ CSL grain boundaries exhibit suppressed Cr RIS segregation, while the RIS response in HAGBs is large. This is because the absorption rate of point defects is dependent on the

grain boundary dislocation density. The exact Σ CSL orientation has the lowest density of dislocation and as the deviation angle increases, the dislocation density increases sharply, which results in the variation of Cr RIS response at different grain boundaries. It suggests that grain boundary engineering is promising to develop steels more resistant to RIS.

Acknowledgement

The authors acknowledge the financial support from The National Natural Science Foundation of China (Grant 51771097, Grant 11705173), The National Magnetic Confinement Fusion Energy Research Project of China (Grant 2015GB118001), The National Key Research and Development Plan (Grant 2017YFB0305201), The Science Challenge Project (Grant TZ2018004), The National Basic Research Programs of China (Grant 2015CB654802).

References

[1] P. Yvon, M. Le Flem, C. Cabet, J.L. Seran, Structural materials for next generation nuclear systems: challenges and the path forward, Nucl. Eng. Des. 294 (2015) 161–169.
[2] S.J. Zinkle, J.T. Busby, Structural materials for fission & fusion energy, Mater. Today 12 (11) (2009) 12–19.
[3] P. Yvon, F. Carré, Structural materials challenges for advanced reactor systems, J. Nucl. Mater. 385 (2) (2009) 217–222.
[4] A. Kostka, K. Tak, R. Hellmig, Y. Estrin, G. Eggeler, On the contribution of carbides and micrograin boundaries to the creep strength of tempered martensite ferritic steels, Acta Mater. 55 (2) (2007) 539–550.
[5] M. Nastar, F. Soisson, Radiation-induced segregation, Compr. Nucl. Mater. 1 (2012) 471–496.
[6] Y. Yang, K.G. Field, T.R. Allen, J.T. Busby, Roles of vacancy/interstitial diffusion and segregation in the microchemistry at grain boundaries of irradiated Fe–Cr–Ni alloys, J. Nucl. Mater. 473 (2016) 35–53.
[7] Z. Lu, R.G. Faulkner, G. Was, B.D. Wirth, Irradiation-induced grain boundary chromium microchemistry in high alloy ferritic steels, Scripta Mater. 58 (10) (2008) 878–881.
[8] J.P. Wharry, G.S. Was, A systematic study of radiation-induced segregation in ferritic–martensitic alloys, J. Nucl. Mater. 442 (1–3) (2013) 7–16.
[9] G.S. Was, J.P. Wharry, B. Frisbie, B.D. Wirth, D. Morgan, J.D. Tucker, T.R. Allen, Assessment of radiation-induced segregation mechanisms in austenitic and ferritic–martensitic alloys, J. Nucl. Mater. 411 (1–3) (2011) 41–50.
[10] K.G. Field, B.D. Miller, H.J.M. Chichester, K. Sridharan, T.R. Allen, Relationship between lath boundary structure and radiation induced segregation in a neutron irradiated 9wt.% Cr model ferritic/martensitic steel, J. Nucl. Mater. 445 (1–3) (2014) 143–148.
[11] R. Hu, G.D.W. Smith, E.A. Marquis, Effect of grain boundary orientation on radiation-induced segregation in a Fe–15.2at.% Cr alloy, Acta Mater. 61 (9) (2013) 3490–3498.
[12] K.G. Field, L.M. Barnard, C.M. Parish, J.T. Busby, D. Morgan, T.R. Allen, Dependence on grain boundary structure of radiation induced segregation in a 9wt.% Cr model ferritic/martensitic steel, J. Nucl. Mater. 435 (1–3) (2013) 172–180.
[13] R.A. Johnson, N.Q. Lam, Solute segregation in metals under irradiation, Phys. Rev. B 13 (10) (1976) 4364–4375.
[14] A.D. Marwick, Calculation of bias due to solute redistribution in an irradiated binary alloy: surfaces of a thin foil, J. Nucl. Mater. 135 (1) (1985) 68–76.
[15] R.C.P.A.D. Marwick, M.E. Horton, Radiation-induced Segregation in Fe-Cr-Ni Alloys, Dimensional Stability and Mechanical Behaviour of Irradiated Metals and Alloys, 1983.
[16] A.D. Marwick, Segregation in irradiated alloys : the inverse Kirkendall effect and the effect of constitution on void swelling, J. Phys. F Met. Phys. 8 (9) (1978) 1849–1861.
[17] P.R. Okamoto, L.E. Rehn, Radiation-induced segregation in binary and ternary alloys, J. Nucl. Mater. 83 (1) (1979) 2–23.
[18] H. Wiedersich, P.R. Okamoto, N.Q. Lam, A theory of radiation-induced segregation in concentrated alloys, J. Nucl. Mater. 83 (1) (1979) 98–108.
[19] S.M. Murphy, Contribution of interstitial migration to segregation in concentrated alloys, J. Nucl. Mater. 182 (1991) 73–86.
[20] S.M. Murphy, J.M. Perks, Analysis of phosphorus segregation in ion-irradiated nickel, J. Nucl. Mater. 171 (2–3) (1990) 360–372.
[21] S.M. Murphy, A model for segregation in dilute alloys during irradiation, J. Nucl. Mater. 168 (1–2) (1989) 31–42.
[22] S.M.M.J.M. Perks, Modelling the Major Element Radiation-Induced Segregation in Concentrated Fe-Cr-Ni Alloys, Materials for Nuclear Reactor Core Applications, 1987.
[23] T.R. Allen, G.S. Was, Modeling radiation-induced segregation in austenitic Fe-Cr-Ni alloys, Acta Mater. 46 (10) (1998) 3679–3691.
[24] T.R. Allen, J.T. Busby, G.S. Was, E.A. Kenik, On the mechanism of radiation-induced segregation in austenitic Fe–Cr–Ni alloys, J. Nucl. Mater. 255 (1) (1998) 44–58.
[25] T.R. Allen, G.S. Was, E.A. Kenik, The effect of alloy composition on radiation-induced segregation in Fe Cr Ni alloys, J. Nucl. Mater. 244 (3) (1997) 278–294.
[26] S. Watanabe, Y. Takamatsu, N. Sakaguchi, H. Takahashi, Sink effect of grain boundary on radiation-induced segregation in austenitic stainless steel, J. Nucl. Mater. 283–287 (2000) 152–156.
[27] T.S. Duh, J.J. Kai, F.R. Chen, L.H. Wang, Numerical simulation modeling on the effects of grain boundary misorientation on radiation-induced solute segregation in 304 austenitic stainless steels, J. Nucl. Mater. 294 (3) (2001) 267–273.
[28] K.G. Field, Y. Yang, T.R. Allen, J.T. Busby, Defect sink characteristics of specific grain boundary types in 304 stainless steels under high dose neutron environments, Acta Mater. 89 (2015) 438–449.
[29] J.P. Wharry, G.S. Was, The mechanism of radiation-induced segregation in ferritic–martensitic alloys, Acta Mater. 65 (2014) 42–55.
[30] G.S. Was, Fundamentals of Radiation Materials Science Metals and Alloys, 2007.
[31] L.D. Xia, W.B. Liu, H.P. Liu, J.H. Zhang, H. Chen, Z.G. Yang, C. Zhang, Radiation damage in helium ion–irradiated reduced activation ferritic/martensitic steel, Nucl. Eng. Technol. 50 (1) (2018) 132–139.
[32] P. Lejcek, Grain Boundary Segregation in Metals, 2010.
[33] Y.N. Osetsky, A. Serra, Vacancy and interstitial diffusion in bcc-Fe, Defect Diffusion Forum 143 (1997) 155–160.
[34] S.J. Rothman, L.J. Nowicki, G.E. Murch, Self-diffusion in austenitic Fe-Cr-Ni alloys, J. Phys. F Met. Phys. 10 (3) (1980) 383–398.
[35] J.P. Wharry, Z. Jiao, G.S. Was, Application of the inverse Kirkendall model of radiation-induced segregation to ferritic–martensitic alloys, J. Nucl. Mater. 425 (1–3) (2012) 117–124.
[36] D.G. Brandon, The structure of high-angle grain boundaries, Acta Metall. 14 (11) (1966) 1479–1484.